A new methodology for thermostructural topology optimization: Analytical definition and validation

A new methodology for thermo-structural topology optimisation: analytical definition and validation

R. Caivano[1,*], A. Tridello[1], M. Codegone[2], G. Chiandussi[1]

[1] Department of Mechanical and Aerospace Engineering, Politecnico di Torino, 10129 Turin, Italy.
[2] Department of Mathematical Sciences 'G. L. Lagrange', Politecnico di Torino, 10129 Turin, Italy.
[*] Corresponding author, riccardo.caivano@polito.it

ABSTRACT

In last few years, the rapid diffusion of components produced through Additive Manufacturing processes has boosted the research on design methodologies based on topology optimization algorithms. Structural topology optimization is largely employed, since it permits to minimize the component weight and to maximize its stiffness and, accordingly, to optimize its resistance under structural loads. On the other hand, thermal topology optimization has been less investigated, even if in many applications, such as turbine blades, engines, heat exchangers, thermal loads have a crucial impact. Currently, structural and thermal optimizations are mainly considered separately, despite the fact that they are both present and coupled in components in service condition. In the present paper, a novel methodology capable to define the optimized structure under simultaneous thermo-mechanical constraints is proposed. The mathematical formulation behind the optimization algorithm is reported. The proposed methodology is finally validated on literature benchmarks and on a real component, confirming that it permits to define the topology which presents maximized thermal and mechanical performance.

KEYWORDS

Thermo-mechanical topology optimization, loop heat pipe (LHP) radiator, Additive Manufacturing (AM)

1. INTRODUCTION

In the last few years, the use of topology optimization algorithms for the design of components for structural applications has significantly increased. A significant boost to the use of optimization design methodologies has been given by the rapid development of Additive Manufacturing (AM) processes, which permit to manufacture complex shapes that were previously hardly producible due to manufacturing constraints.

Topology optimization algorithms are currently used to reliably design components subjected to static mechanical loads such as brackets, supports, anchors. One of the most used method is SIMP (Solid Isotropic Microstructure with Penalization for intermediate densities) which employs a density variable and a penalization exponent to locally "penalize" the stiffness and avoid elements with intermediate densities (1). Other methodologies widely employed in the

literature are the BESO (Bidirectional Evolutionary Structural Optimisation) (2) and the LS (Level Set) approach (3). The first approach adds and removes elements depending on their strain energy densities. The second approach uses a higher order function, namely level set function, whose zero values correspond to the boundary of the optimised structure. A comparative review of the most common structural topology optimisation approaches can be found in (4).

Similarly, thermal topology optimization was investigated in the literature and algorithms that permit to maximize conduction heat transfer in the material have been proposed. Most of them are analysed and reviewed by Dbouk in (5). An experimental investigation of this type of topology optimisation is provided by Subramainam in (6). It is worth to note that the optimisation strategies are the same employed for the enhancement of the mechanical stiffness. For example, Gersborg-Hansen et al. (7) applied the SIMP strategy to the heat conduction topology optimisation and Gao et al. (8) employed the BESO method with the same aim.

Nevertheless, some components in real applications can be subjected to combined structural and thermal loads, like as turbine blades, engines or heat exchangers. Consequently, the development of optimization algorithms allowing to design structures subjected to coupled thermal and structural loads is of utmost interest among researchers and industry.

These algorithms can be divided in two main categories. The first one consists of a classical stiffness maximisation considering the effect of the induced thermal stress and strains. In other words, the structural topology optimisation must consider the presence of a temperature field which modifies the strain distribution. For examples, Zhu et al. (9) presented a temperature-constrained topology optimization method for thermo-mechanical coupled problems. Tong at al. (10) proposed a multiple material topology optimisation under the conditions of steady-state temperature and mechanical loading. Deaton at al. (11) presented a method for topology optimization of structures with combined mechanical and thermoelastic (temperature) loads subjected to stress constraints. Zhang et al. (12) proposed a mean compliance and elastic strain energy minimization for thermoelastic problems. Lastly, Liu et al. (13) presented a guide-weight method to solve the topology optimization problems of thermoelastic structures.

The second category of algorithms for thermo-structural optimization problems consists of methods aimed to find the final topology which maximise/minimize the heat exchange and maximise structural stiffness. Therefore, the objective function is no more purely mechanical but must also take into account thermal objective, such as guarantee a defined heat exchange. For example, Yang at al. (14) defined a topology optimisation method that consider both thermal and mechanical objectives. Takezawa et al. (15) proposed a topology optimization algorithm with constraints on structural strength and thermal conductivity. Krysko et al. (16) presented method for the topology optimization of the microstructure of a composite material with the aim of finding the material with the most effective values of the bulk modulus of elasticity and

thermal conductivity. Deng et al. (17) developed a hybrid cellular automaton model combined with finite element method for structural topology optimization with mechanical and heat constraints.

According to the literature, thermo-mechanical topology optimisation has been widely investigated and there are many publications in this area. However, further improvements in this field can be achieved. First, the majority of the algorithms is based on SIMP or RAMP (Rational Approximation Material Properties) approaches which require a penalisation factor. This factor is often linked with convergence problems such as local minima which require different corrections techniques (18). Considering evolutionary methods, such as BESO, a lack of an analytical generality and convergence criteria has been observed, as stated in (4). Furthermore, if the objective function and the constraints are fairly complex, the formulated optimisation problem often needs advanced programming methods such as MMA (Method of Moving Asymptotes) (19) and sensitivity analysis to be solved.

In the present paper, an innovative methodology for the maximization of the thermal exchange and the mechanical stiffness of a structure under thermo-mechanical loads is proposed. Differently from the literature, penalisation factors are not required and there is no need of numerical corrections. In addition, a simple formulation for the optimality criteria is analytically derived and physically verified. The proposed objective function parametrisation allows to analytically solve the optimisation problem, i.e. numerical programming methods and sensitivities analysis are not required. The stresses induced by the thermal loads are considered in the optimisation and the thermal exchange and the structural stiffness are concurrently optimized, thus permitting to assess a more effective material distribution.

In the first part of the paper, the analytical formulation of the problem is reported and solved and the criteria for the global optimum are defined. Thereafter, the proposed algorithm is validated with several benchmark and applicative examples. Finally, a real component employed for aerospace applications is thermo-mechanically optimised, proving the applicability and effectiveness of the presented method.

2. METHODS

In this Section the analytical formulation of the proposed methodology is reported. In particular, in Subsection 2.1 optimality criteria for a system subjected to thermo-structural loads are defined and in Subsection 2.2 the flow chart of the proposed algorithm is reported and described. In the following **bold** letters stand for vector quantities.

2.1 Thermo-structural topology optimization: the optimality criteria

The current topology optimization formulation provides a method allowing to assess the best material exploitation for a component subjected to structural and thermal loads. In particular, the heat exchange and the mechanical stiffness are maximized at the same time. In order to achieve this goal, the expression of the potential energy of the system has to be obtained and then the structural optimisation problem consists in its minimization under selected constraints. In other words, through the minimization of the potential energy, the component deformation is minimized while the stiffness is maximized.

The starting point of the proposed optimization method is the equilibrium equation for a system subjected to thermo-mechanical loads, shown schematically in Fig. (1a). Let consider as domain of existence a portion of a system Ω limited in the space ($\Omega \subseteq \mathbb{R}^3$) containing the material M, with regular frontier Γ. The spatial coordinates are called x, y, z or, in vector notation, $\boldsymbol{x}$. The displacement field of M is $\boldsymbol{u} = \boldsymbol{u}(\boldsymbol{x})$ and the temperature field is $\theta = \theta(\boldsymbol{x})$. The material M is assumed to be isotropic with a linear elastic behaviour (i.e., it follows the Hooke's law (20)) and it is characterized by Young's modulus E, Poisson's ratio ν, thermal expansion coefficient α, thermal conductivity k and density ρ. In addition, all the applied boundary conditions satisfy the border completeness (21), according to Eq. (1). In other words, each portion of the frontier Γ is defined by a boundary condition, both thermal and structural:

$$\begin{aligned} \Gamma_N^{\theta} \cup \Gamma_D^{\theta} = \Gamma \quad and \quad \Gamma_N^{\theta} \cap \Gamma_D^{\theta} = \emptyset \\ \Gamma_N^{\boldsymbol{u}} \cup \Gamma_D^{\boldsymbol{u}} = \Gamma \quad and \quad \Gamma_N^{\boldsymbol{u}} \cap \Gamma_D^{\boldsymbol{u}} = \emptyset \end{aligned} \tag{1}$$

where Γ_N^{θ} is the Neumann boundary condition of the thermal field, Γ_D^{θ} is the Dirichlet boundary condition of the thermal field, Fig. (1c), Γ_N^{u} is the Neumann boundary condition of the structural field and Γ_D^{u} is the Dirichlet boundary condition of the structural field (Fig. (1c)). The symbol ∅ stands for empty set.

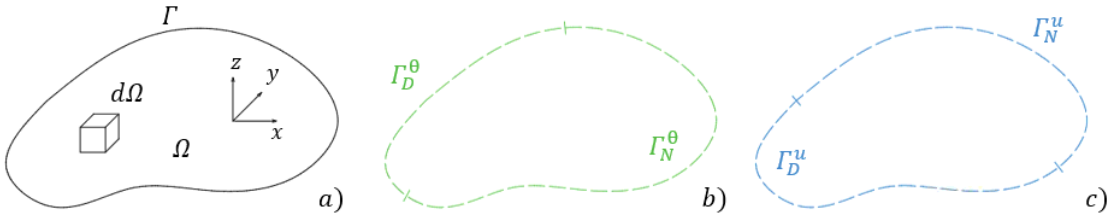

Figure 1 – Thermo-mechanical system: a) domain Ω, infinitesimal portion $d\Omega$, regular frontier Γ, coodinate system $x - y - z$; b) thermal boundary conditions Γ_N^{θ}, Γ_D^{θ}; c) mechanical boundary conditions Γ_N^{u}, Γ_D^{u}.

The overall equilibrium of an infinitesimal portion $d\Omega$ of the system Ω is described by Eq. (2), as reported in (21).

$$\begin{bmatrix} \boldsymbol{\nabla\sigma} & \beta\boldsymbol{\nabla} \\ \boldsymbol{0}^T & k\boldsymbol{\nabla^2} \end{bmatrix} \begin{pmatrix} \boldsymbol{u} \\ \theta \end{pmatrix} + \begin{pmatrix} \boldsymbol{F} \\ H \end{pmatrix} = \boldsymbol{0} \tag{2}$$

in which $\boldsymbol{\nabla}$ is the operator of derivation with respect to the three space dimensions, $\boldsymbol{\nabla^2}$ is the Laplacian operator, β is the thermo-mechanical coupling term (i.e., equal to the product of the Young's modulus E and the thermal expansion coefficient α, $\beta = E\alpha$), k is the thermal conduction coefficient, $\boldsymbol{\sigma}$ is the stress tensor, $\boldsymbol{F}$ is the vector of internal forces, H is the internal generated heat and $\mathbf{0}$ is the null vector. Applying the variational methodology as done in (22), by integrating Eq. (2) in the domain Ω, it is possible to obtain the weak expression of the potential energy of the system. In particular, the solution of a thermo-mechanical topology optimization problem can be achieved by implementing the weak expression of the potential energy by excluding differential terms. The resulting potential energy equation is a scalar quantity and corresponds to the *thermo-mechanical potential energy,* $\Pi(\boldsymbol{u}, \theta)$ of the system shown in Eq. (3):

$$\Pi(\boldsymbol{u}, \theta) = -\frac{1}{2}\left(\int_{\Omega} \boldsymbol{e}^T(\boldsymbol{u})\boldsymbol{A}\boldsymbol{e}(\boldsymbol{u})\, d\boldsymbol{x} \; + \xi \int_{\Omega} k\nabla^2\theta \, d\boldsymbol{x} + \int_{\Omega} \beta \, \nabla^T\theta \; \boldsymbol{u} \; d\boldsymbol{x}\right) \tag{3}$$

where the term $\boldsymbol{e}$ is the vector of the structural deformations or strains**,** $\boldsymbol{A}$ is the constitutive matrix**.** The term ξ represents the linker between thermal and mechanical energy (measure unit [time/temperature]). It allows to consider in the same potential equation both the contributes without violating physical continuity. ξ must be chosen in order to balance the structural and the thermal contributes, assigning therefore the same importance to each contribution. It has to be evaluated according to the design constraints before the optimization process (see Section 3).

Eq. (3) is the objective function that must be minimised in order to find the optimal topology. A system that a has smaller coupled potential energy is subjected to smaller variations of its state, i.e. temperature and displacement. In order to define the optimisation problem, it is necessary to define an artificial variable, called η. This variable represents the material effectiveness in each point of the domain Ω. In other words, η stands for the presence and consistency of the material in the domain, point by point. The variable η must be limited both by an upper boundary η_{max} and by a lower boundary η_{min} (23).

$$\begin{gathered} \eta = \eta(\boldsymbol{x}) \\ 0 < \eta_{min} < \eta < \eta_{max} < \infty \end{gathered} \tag{4}$$

For $\eta = \eta_{max}$ the material is considered full, so the material properties are the same of the base material M, for $\eta = \eta_{min}$ the material considered void and its properties are close to be null.

The topology optimisation problem, reported in Eq. (5), consists in finding the distribution of $\eta(\boldsymbol{x})$ that minimises the coupled potential energy $\Pi(\boldsymbol{u},\theta)$ for a volume $\overline{W}$. $\overline{W}$ is a portion of the initial volume and the second equation in Eq. (5) represents the volume optimisation constraint.

$$\begin{cases} \max_{\eta} \Pi(\eta,\boldsymbol{u},\theta) = \min_{\eta} \frac{1}{2}\left(\int_{\Omega} \boldsymbol{e}^T(\boldsymbol{u})\boldsymbol{A}\boldsymbol{e}(\boldsymbol{u})\,\eta\,d\boldsymbol{x} + \xi\int_{\Omega} k\nabla^2\theta\;\eta\,d\boldsymbol{x} + \int_{\Omega}\beta\,\nabla^T\theta\;\boldsymbol{u}\,\eta\,d\boldsymbol{x}\right) \quad s.t. \\ \int_{\Omega}\eta\,d\Omega \le \overline{W} \\ 0 < \eta_{min} < \eta < \eta_{max} < \infty \end{cases} \tag{5}$$

The optimization problem in Eq. (5) can be solved by iteratively applying Kuhn-Tucker optimality criteria (Lagrange multiplier method,(23)). In particular, the Lagrangian function $L(\eta,\lambda,t)$, has to be defined and all its derivatives must be equal to zero (Eq. (6)) in order to identify a stationary point of the function:

$$L(\eta,\boldsymbol{\lambda},t) = \frac{1}{2}\left(\int_{\Omega} \boldsymbol{e}^T(\boldsymbol{u})\boldsymbol{A}\boldsymbol{e}(\boldsymbol{u})\,\eta\,d\boldsymbol{x} + \xi\int_{\Omega} k\nabla^2\theta\,\eta\,d\boldsymbol{x} + \int_{\Omega}\beta\,\nabla^T\theta\;\boldsymbol{u}\,\eta\,d\boldsymbol{x}\right) - \lambda\left(\int_{\Omega}\eta\,d\Omega - \overline{W} + t^2\right) \tag{6}$$

where λ is a *Lagrange multiplier* and the term t is an additional variable employed to simplify the solution of the system. By equalling to zero the first derivative of the Lagrangian function, λ becomes the *thermo-mechanical energy density* ϵ, with the expression reported in Eq. (7).

$$\lambda = \frac{\frac{1}{2}\left(\int_{\Omega} \boldsymbol{e}^T(\boldsymbol{u})\boldsymbol{A}\boldsymbol{e}(\boldsymbol{u})\,d\boldsymbol{x} + \xi\int_{\Omega} k\nabla^2\theta\,d\boldsymbol{x} + \int_{\Omega}\beta\,\nabla^T\theta\;\boldsymbol{u}\;d\boldsymbol{x}\right)}{\int_{\Omega} d\Omega} = \epsilon \tag{7}$$

If the problem is discretized by using k elements, e.g. using the Finite Element Method (FEM), Equation (7) is defined on each k portion of the domain called Ω_i and the effectiveness variable η must be discretised too.

$$\begin{cases} \eta(\boldsymbol{x}) = \eta_i \quad \forall \boldsymbol{x} \in \Omega_i \quad i = 1,\dots,k \\ 0 < \eta_{min} < \eta_i < \eta_{max} < \infty \end{cases} \tag{8}$$

Following the same passages shown in Eqs. (3)-(7), the value of the *Lagrange multiplier* for each element can be evaluated as follows:

$$\lambda_i = \frac{\frac{1}{2}(\boldsymbol{e_i}^T(\boldsymbol{u})\boldsymbol{A}\boldsymbol{e_i}(\boldsymbol{u}) + \xi\nabla_i^T\theta k(\boldsymbol{x})\nabla_i\theta + \beta\,\nabla_i^T\theta\;\boldsymbol{u_i})\Omega_i}{\Omega_i} = \epsilon_i = \lambda = \epsilon \quad i = 1,\dots,k \tag{9}$$

The Lagrange multiplier for each element corresponds therefore to the thermo-mechanical energy density for that element. According to (23), the Lagrange multiplier must be the same for the entire structure, thus every λ_i needs to be equal to the value found by considering a continuous solution (i.e., $\lambda = \lambda_i$, with λ defined according to Eq. (7)). Therefore, the thermo-mechanical energy density in each element has to be uniformly distributed within the structure in the optimized topology (optimality criteria). The assessment of the material distribution ensuring a uniform thermo-mechanical energy density is therefore the objective of the optimization algorithm proposed by the Authors. For more, the optimisation problem as formulated is convex since no material interpolation is employed (18). Therefore, the proposed methodology guarantees that a global minimum for the thermo-mechanical topology optimisation problem is achieved.

2.2 Iterative algorithm for the thermo-structural topology optimization

The flowchart in Fig. (2) shows the iterative optimisation process developed to obtain the optimized topology, i.e. a uniformly distributed thermo-mechanical energy density.

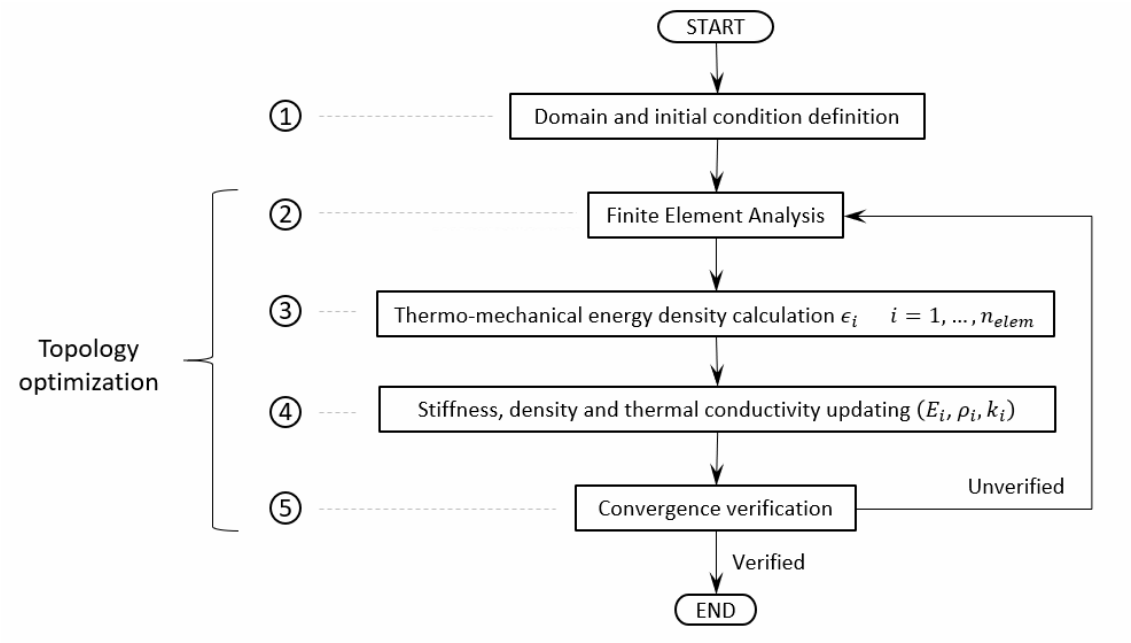

Figure 2 - Flow chart of thermo-mechanical topology optimisation.

The preliminary phase is the definition of the Finite Element Model and the initial conditions, which corresponds to phase number 1 in Fig. (2). Then phase number 2 consists of a FE simulation on the initial model. This simulation allows to evaluate the distribution of the thermal gradient and mechanical strain. These quantities are used to calculate the thermo-mechanical energy density ϵ_i for each element as shown in Eq. (9) and it represents step number 3 in Fig.

(2). The 4th phase corresponds to the update of the local properties of material, i.e. Young's modulus, density and thermal conductivity. This procedure is the main core of the optimisation process and it allows to obtain the final material distribution. It is possible to achieve a final topology that ensures the uniform distribution of the thermo-mechanical energy density by modifying the local properties of the material according to a precise updating law. This updating law can be achieved considering the effectiveness of the material together with Eq. (9) as done by (23). Eq. (10) expresses the relationship between the local effectiveness and the thermo-mechanical energy density. It is worth to note that the updating process is iterative, this is because the effectiveness variable is limited as stated in Eqs. (4) and (8), and the modification of this variable causes the variation of the thermal gradient and mechanical strain distribution (23). Therefore, in Eq. (10) index j refers to a single iteration while p is its total number.

$$\eta_i^{j+1} = \frac{\epsilon_i^j}{\epsilon^j}\eta_i^j \qquad i = 1, \dots, k \quad j = 1, \dots, p \tag{10}$$

In the previous equation, considering element i and iterations j and $j+1$, η_i^{j+1} is the updated effectiveness, η_i^j is the current one, while ϵ_i^j represents the thermo-mechanical energy density for the element and ϵ^j stands for the average thermo-mechanical energy density in the global structure.

In order to link the artificial material effectiveness variable to the real parameters of the material, η_i is considered multiplying the Young's modulus E_i, the density ρ_i and the thermal conductivity k_i as shown in Eq. (11). The material properties and the material effectiveness η with the subscript i refer to a single element considered for the discretization of the domain and vary during each iteration, whereas the material properties of the base material, indicated with the subscript 0 in Eq. (11), remain constant (i.e., E_0, k_0 and ρ_0 stand respectively for the Young's modulus, the density and the thermal conductivity of the material at the beginning of the process):

$$\eta_i = \frac{E_i}{E_0} = \frac{k_i}{k_0} = \frac{\rho_i}{\rho_0} \quad i = 1, \dots, k$$
$$0 < 10^{-4} \div 10^{-5} \leq \eta_i \leq 1 < \infty \quad i = 1, \dots, k \tag{11}$$

A good approximation for η_{min} is around 10^{-4} to 10^{-5} (23). Finally, the updating law for the material parameters employed in step 4 is shown in Eq. (12).

$$\begin{cases} E_i^{j+1} = \dfrac{\epsilon_i^j}{\epsilon^j} E_i^j \\ \rho_i^{j+1} = \dfrac{\epsilon_i^j}{\epsilon^j} \rho_i^j \\ k_i^{j+1} = \dfrac{\epsilon_i^j}{\epsilon^j} k_i^j \end{cases} \qquad i = 1, \dots, k \quad j = 1, \dots, p \tag{12}$$

During the iterative procedure, the elements of the material that participate scarcely to the load sharing are characterized by a low energy density, hence their effectiveness is reduced, i.e. the density, the Young's modulus and the conductivity of the element are lowered and vice versa. In order to define when the final topology has been achieved, a convergence criterion of the iterative process is needed. This represents phase 5 in Fig. (2). The convergence occurs when the change in the variables is less than the imposed convergence parameter, usually less than 1 percent. At this condition corresponds a discrete distribution of material, i.e. full or void material without intermediate values. This criterion is the same used by O. Sigmund in (24). It is possible to verify the volume constraint imposing a certain value to the Lagrange multiplier in Eq. (9) using a bi-sectioning algorithm.

Another convergence criterion is proposed in (23). In particular, the volume constraint can be considered in term of reference energy. In this case, an objective thermo-mechanical energy density in the structure ϵ_{ref} is defined before the optimization process. For example, ϵ_{ref} can be defined by considering the maximum allowable stress within the structure and the maximum allowable thermal gradient. The convergence is reached if the percentage difference between ϵ_{ref} and the average thermo-mechanical energy density $\overline{\epsilon}$ evaluated in the structure is lower than 0.1% for three consecutive iterations. This criterion considers concurrently the changing of the variables and the energy constraint.

Depending, on the application and on the final objective of the optimization process, these two criteria can be alternatively considered.

3. RESULTS

In this section, the proposed optimisation algorithm is validated. In particular, in Subsection 3.1 the proposed algorithm is verified by considering two bidimensional literature benchmarks and in Subsection 3.2 it is validated on a three-dimensional component used for aerospace applications.

For the implementation of the proposed algorithm, the commercial software Ansys has been used. In particular, a routine has been written in the Ansys APDL software for iteratively assessing the stress and the thermal gradients for each element and thereafter updating the material properties until the convergence criterion is met, according to flow-chart in Fig. (2).

In particular, the 1st phase is implemented simply coding the geometry settings and boundary conditions of the initial domain in APDL code. The 2nd phase, consisting of the finite element analyses, is processed by the solution command. Automatically, all the results information is achieved, i.e. stresses, strains, displacements, energies and so on. At this point, it is possible to evaluate the thermo-mechanical energy density for each element through Eq. (9), namely the 3rd phase. Given this coupled energy density for each element, it is possible to update the material parameters of each element following Eq. (12). In particular, since the energy reference criterion is employed, the term ϵ^j is substituted with ϵ_{ref}. Therefore, the elements which have an energy density lager than the reference will be rewarded. On the other hand, if the energy density is smaller than the reference value, the element is penalized. Therefore, only the elements which are most meaningful for the load bearing purpose are selected in the final topology. After that, the updated material parameters are cut according to the minimum and maximum value imposed in Eq. (11). This updating procedure refers to the 4th phase. At this point, the convergence criterion can be checked as stated in the 5th phase. Since in the following cases a reference thermo-mechanical energy density is imposed, the convergence can be considered reached when the average thermo-mechanical energy density matches the reference one for three consecutive iterations. At this condition corresponds a discrete distribution of material, i.e. full or void material without intermediate values of the material properties. This means also that each element shares in average the same ϵ_{ref} and the updating law in Eq. (12) is no more effective. All the described processes can be easily coded in less than 150 code lines in APDL.

3.1 2D literature benchmark validation

A beam with length $L = 200\ \mathrm{mm}$, height $h = 100\ \mathrm{m}$, with mechanical and thermal loads applied concurrently was considered for the validation of the proposed algorithm. In every bidimensional case considered, the plane stress assumption has been employed. In the first case, shown in Fig. (3a), the beam is simply supported with a vertical force $F = 1000\ N$ applied in the middle of the lower edge. In addition, a portion of each edge with length $d = 10\ \mathrm{mm}$, symmetric with respect to the beam axes presents a fixed constant temperature. On the horizontal edge portions (shown in red in Fig. (3a)) the imposed temperature, T_1, is equal to $100°C$, whereas it is equal to $0°C$ on the vertical edge portions (T_2, shown in blue in Fig. (3a)). In the second case, shown in Fig. (3b), the beam is fixed at the left edge (cantilever beam condition), with a vertical force F applied at the right end. Thermal loads are represented by the constant temperature T_1 along the entire left edge and an outgoing heat flow $Q = 1W$ (according to Fig. (3b)) applied on a central portion d of the right vertical edge. A common steel

was considered for the constitutive model of the material and its properties are reported in Table 1. Plane square quad 8 nodes elements, with the side length of 1 mm, were employed for the analysis. For a detailed description of element definition, the reader is referred to ANSYS guide manual to element PLANE 223.

Material	E [GPa]	ν	ρ [Kg/m^3]	k [W/mK]	α [1/K]
Steel	210	0.3	7800	50	12e-6

Table 1 –Properties of the steel considered for the validation of the benchmarks

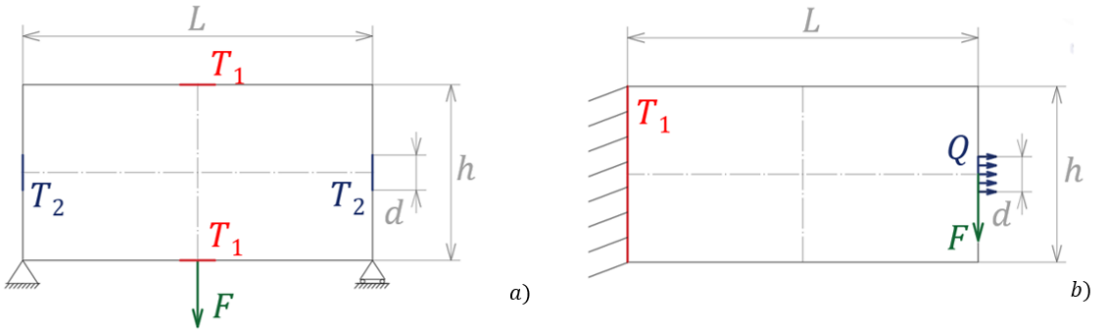

Figure 3 – Validation of the proposed algorithm on a 2D domain: a) simple supported beam with different fixed temperatures, b) cantilever beam with fixed temperature and outgoing heat flow. $L = 200$ mm , $h = 100$ mm, $d = 10$ mm , $F = 1000$ N , $T_1 = 100$°C, $T_2 = 0$°C, $Q = -1$W.

The convergence criterion was thereafter defined. In particular, a reference thermo-mechanical energy density ϵ_{ref} (convergence criterion) evaluated as a balanced sum between the reference strain energy density ϵ_{ref}^{σ} and the reference thermal energy density ϵ_{ref}^{θ} was considered.

$$\epsilon_{ref} = \epsilon_{ref}^{\sigma} + \xi\epsilon_{ref}^{\theta} \tag{13}$$

This separated reference energy densities ϵ_{ref}^{σ} and ϵ_{ref}^{θ} can be calculated according to (23). In particular, ϵ_{ref}^{σ} can be computed as function of a reference stress σ_{ref} (for example the maximum allowable stress within the component with the formula $\epsilon_{ref}^{\sigma} = \sigma_{ref}^2/2E$), whereas ϵ_{ref}^{θ} can be calculated as a function of a reference thermal gradient $\nabla\theta_{ref}$ (i.e., in order to limit the maximum temperature within the component with the formula $\epsilon_{ref}^{\sigma} = k\nabla\theta_{ref}^2/2$). In particular, for the simply supported beam, σ_{ref} was chosen equal to $60\ MPa$ and $\nabla\theta_{ref} = 0.825\ K/mm$, whereas for the cantilever beam $\sigma_{ref} = 120\ MPa$ and $\nabla\theta_{ref} = 1.1\ K/mm$. These values have been chosen as samples for reference thermal gradient and mechanical stress. As a matter of fact, any value could be employed to run the optimisations. The only limit is to use values that can be reasonable for the employed materials, e.g. reference stress inferior

to the material yield strength. Clearly, different values of these references would bring to different final topologies which would represent the optimal material distributions for that specific case. The linker term ξ can be evaluated with the formula $\xi = \sigma_{ref}^2 / Ek\nabla\theta_{ref}^2$ which guarantees the same weight to both thermal and structural reference contribution. As already stated, this term allows combining the mechanical and the thermal energy. A random value of this linker term may artificially increase the thermal contribute or vice versa. This term must be chosen to balance the two energy contributions. Hence, the reason why this term must be evaluated with this formula can be easily understood by analysing the possible scenarios during the optimisation. For an element characterized by only a structural task, i.e. ϵ^{θ} is null, the thermo-mechanical energy density of this element would be identical to the strain energy density. Vice versa, if the element had only a thermal task, i.e. ϵ^{σ} is null, the thermo-mechanical energy density of this element would be equivalent to the thermal energy density. Hence, in both the extreme situations the numerical value of the coupled energy must be the same. If not, an element with the only thermal task would be considered differently with respect to another with only mechanical one. Therefore, in the end, the topology would be affected by a disparity in task contribute and the final material distribution would foster much more one of them. Choosing the linker term as $\xi = \sigma_{ref}^2 / Ek\nabla\theta_{ref}^2$ this condition is avoided. This consideration is valid for all the intermediate conditions too. Both the thermal and mechanical tasks are kept equally into consideration. For different values of ξ, it would be as if the thermal or structural references would be set to different values from the prescribed ones. The reference thermo-mechanical energy densities ϵ_{ref} for the two cases were finally respectively $\epsilon_{ref}^1 = 1.17 \cdot 10^{-2}\ \mathrm{MPa}$ (for the simply supported beam) and $\epsilon_{ref}^2 = 6.86 \cdot 10^{-2}\ \mathrm{MPa}$ for the cantilever beam.

The results of the optimization process are shown in Fig. (4a) for the simply supported beam with fixed temperatures and in Fig. (4b) for the cantilever beam with fixed temperature and outgoing heat flux. The thermo-mechanical energy density convergence plots for load case 1 and load case 2 are reported in Fig. (4c) and (4d) respectively. As it can be seen, the curves both converge fairly fast to the prescribed reference value. In both cases the convergence is reached with less than 40 iterations.

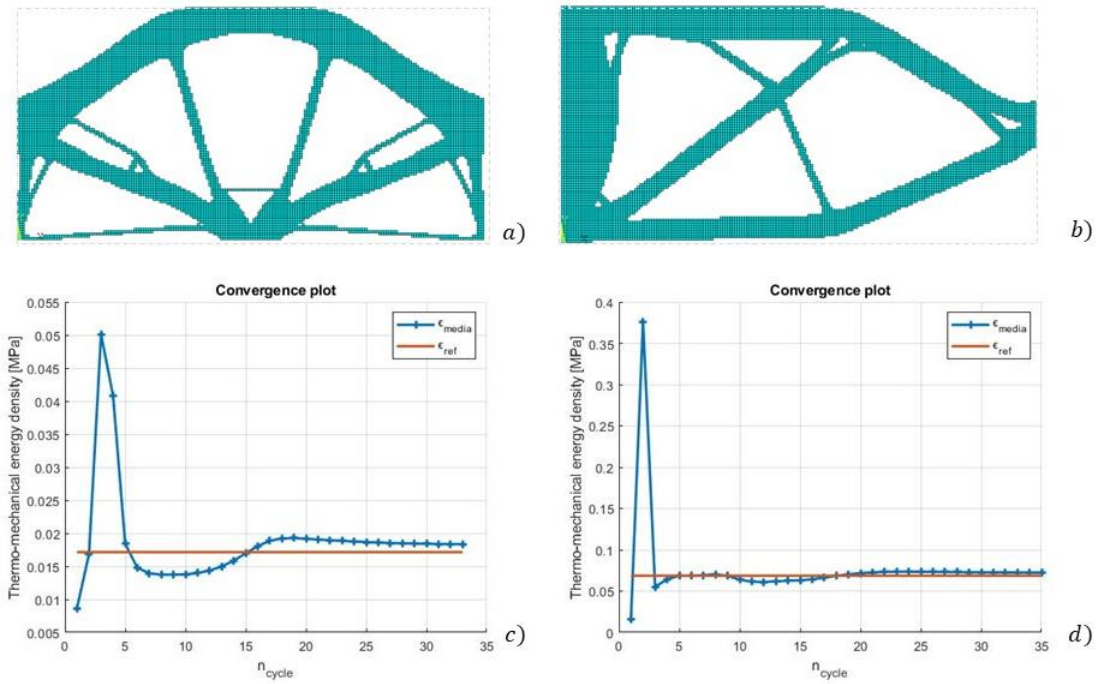

Figure 4 - Final optimised topologies obtained with the proposed thermos-structural algorithm: a) thermo-mechanical load case 1, b) thermo-mechanical load case 2, c) energy density convergence plot for load case 1, d) energy density convergence plot for load case 2.
$\sigma^1_{ref} = 60\ MPa$, $\sigma^2_{ref} = 120\ MPa$, $\nabla\theta^1_{ref} = 0.825\ K/mm$,$\nabla\theta^2_{ref} = 1.1\ K/mm$,
$\xi = \sigma^2_{ref}/Ek\nabla\theta^2_{ref}$, $\epsilon^1_{ref} = 1.17 \cdot 10^{-2}\ MPa$ and $\epsilon^2_{ref} = 6.86 \cdot 10^{-2}\ MPa$.

Fig. (5) shows the distribution of the thermo-mechanical energy density for the simply supported beam Fig. (5a) and for the cantilever beam Fig. (5b). As it can be seen, this quantity has a range of variability almost uniform around the central reference value, according to Eq. (9). This means that in the final topology all the elements bear equally the thermo-mechanical loads, with the material fully exploited and no inactive elements. It is worth to note that some grey zones are present in the Fig. (5). However, these figures have been shown mainly to highlight the uniform distribution of the energies, stress and gradients around the reference values. Indeed, since the loads are applied only on single nodes, nearby this points the stresses and the energies are extremely high. This is due to the fact that the process is numerical, and these extremely large values have not a real physical meaning. If the range from the maximum to the minimum value was considered, almost the whole structure would be characterized by the same colour. This would have avoided grey zones, but it would have not permitted to recognize the slighter variations of the plotted quantity within the domain, which is the real objectives of the figures.

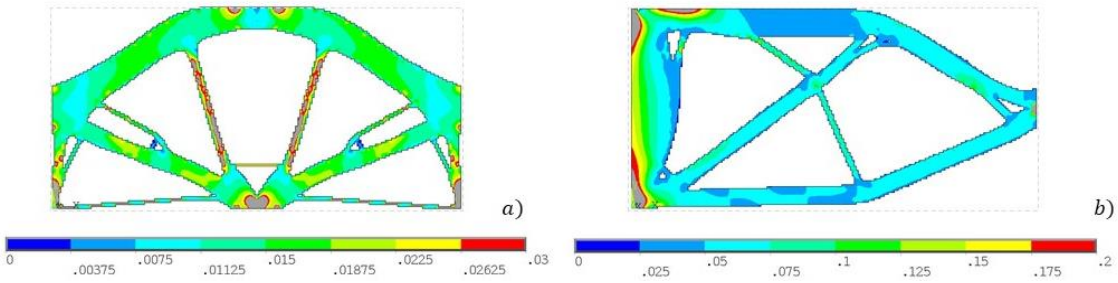

Figure 5 - Thermo-mechanical energy density distribution [MPa]: a) simply supported beam 1, b) cantilever beam.

Fig. (6a)-(6b) show respectively the global displacement and temperature field for the topology obtained in Fig. (4a). As it can be seen, they are both limited and within a reasonable range. Moreover, Fig. (6c)-(6d) show the distribution of Von Mises ideal stress and thermal gradient for the same case, respectively. It is worth to note, that the prescribed references for the stress and thermal gradient were not the maximum allowable ones. Instead, they represent the values at which the average stress and thermal gradient must converge in order to achieve a uniform energy density distribution as done in (23). From a practical point of view, since the zones with the stress exceeding the reference stress are limited, they can be eliminated when the component is "reconstructed" to generate the .cad or the .stl file with the appropriate fillets or with a subsequent shape optimization. Moreover, a larger safety factor can be also considered for reducing the areas with stress larger than the reference stresses.

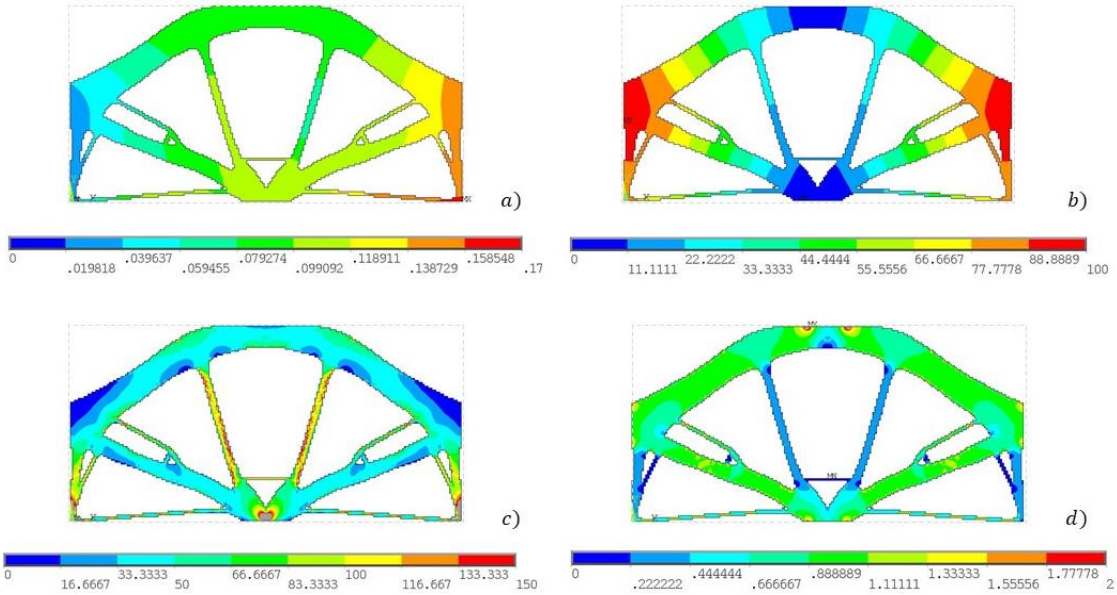

Figure 6 – Meaningful quantities after thermo-mechanical topology optimisation of load case 1: a) displacement vector sum [mm], b) temperature field [°C], c) Von Mises ideal stress [MPa], d) Thermal gradient vector sum [°C/mm].

The same considerations are valid for the cantilever beam. Fig. (7a)-(7b) show the global displacement and temperature field respectively and they are limited as for the previous case. In Figs. (7c)-(7d) the Von Mises ideal stress and the thermal gradient are shown. As before, it is possible to observe that both the quantities are almost uniform around the reference values within the final domain, thus proving that the material is fully exploited.

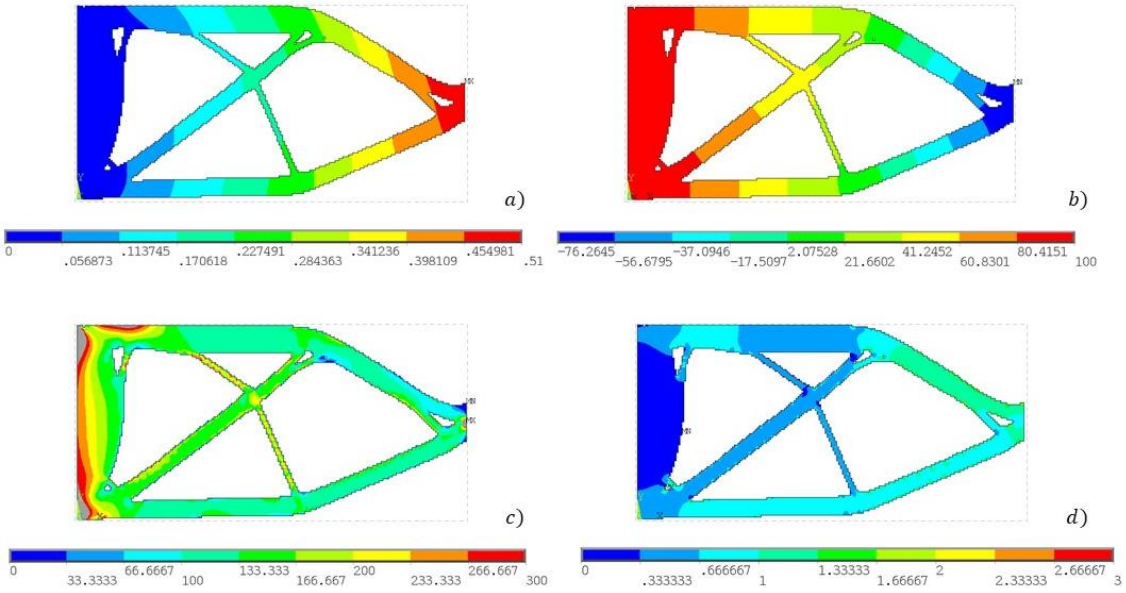

Figure 7 - Meaningful quantities after thermo-mechanical topology optimisation of load case 2: a) displacement vector sum [mm], b) temperature field [°C], c) Von Mises ideal stress [MPa], d) Thermal gradient vector sum [°C/mm].

For the sake of comparison and to highlight the importance of concurrently considering the mechanical and the thermal loads during the optimization process, structural topology optimisations and thermal topology optimization were run separately on the presented load cases. It is important to note that the load cases remain the same reported in Fig. (3). Hence, the boundary conditions are both mechanical and thermal. However, in the following cases the objective function neglects the structural objective or the thermal one. As it will be demonstrated, by considering only the structural or the thermal objective in components subjected to both types of loads, the resulting topology is characterized by a slightly larger effectiveness for the selected objective (thermal or structural depending on the objective of the optimization) but by a limited effectiveness for the neglected functionality. Therefore, this may lead to null heat conduction or overloaded structure. Fig. (8a) shows the final topology obtained for the load case 1 by considering only the structural reference ($\sigma_{ref} = 60$ MPa). Fig. (8b) and Fig. (8c) show the Von Mises stress and the thermal gradient, respectively. By considering Fig. (8b), the stress distribution is uniform, with the same maximum value found through the

coupled thermo-structural topology optimization, ensuring a very good exploitation of the material in terms of mechanical loads. Nevertheless, the thermal gradient, Fig. (8c), results to be almost null over the domain, basically there is no thermal conduction. This happens because the algorithm focuses on the structural task and neglects the thermal one. Therefore, as in this case, only the portion of material important for the structural task are selected. Since they do not coincide with portion of material which guarantee the heat conduction, the thermal gradient results to be almost null over the domain. That's why considering a real application, the component would not be able to guarantee a sufficient heat flow.

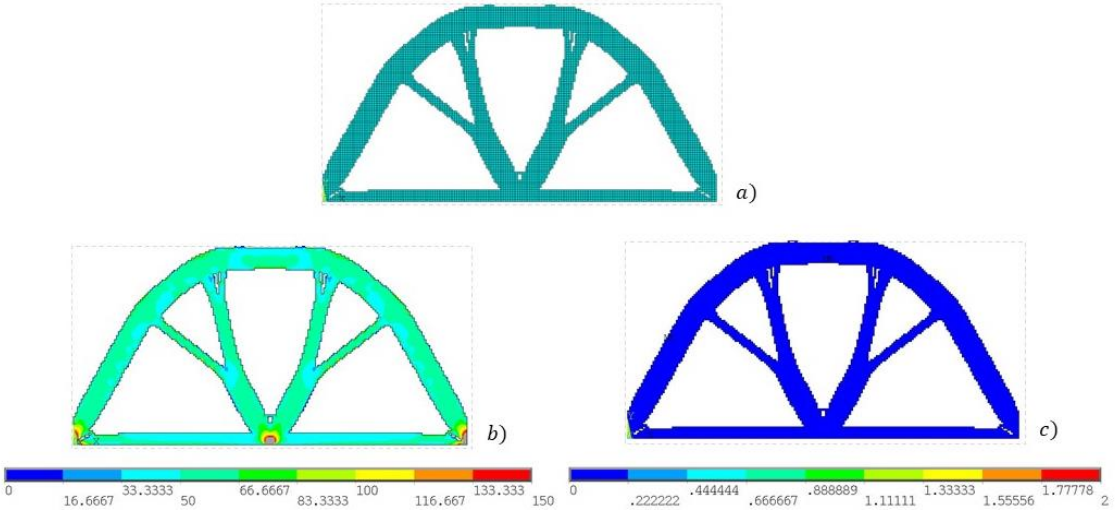

Figure 8 - Meaningful quantities after structural topology optimisation of load case 1: a) final topology, i.e. material distribution b) Von Mises ideal stress [MPa], c) Thermal gradient vector sum [°C/mm].

Fig. (9a) shows the thermal topology optimisation carried out on the load case 1, with $\nabla\theta_{ref} = 0.825\ \mathrm{K/mm}$, whereas Fig. (9b) shows the Von Mises stress distribution and Fig. (9c) the thermal gradient sum. In this case the thermal gradient is uniform over the domain providing a very good thermal conduction. On the other hand, according to Fig. (9c) the Von Mises stress distribution significantly increases by considering only the thermal task, being almost four time greater than in the thermo-mechanical topology optimisation, Fig. (6c). This could bring to possible static failure in the component or faster crack initiation and propagation.

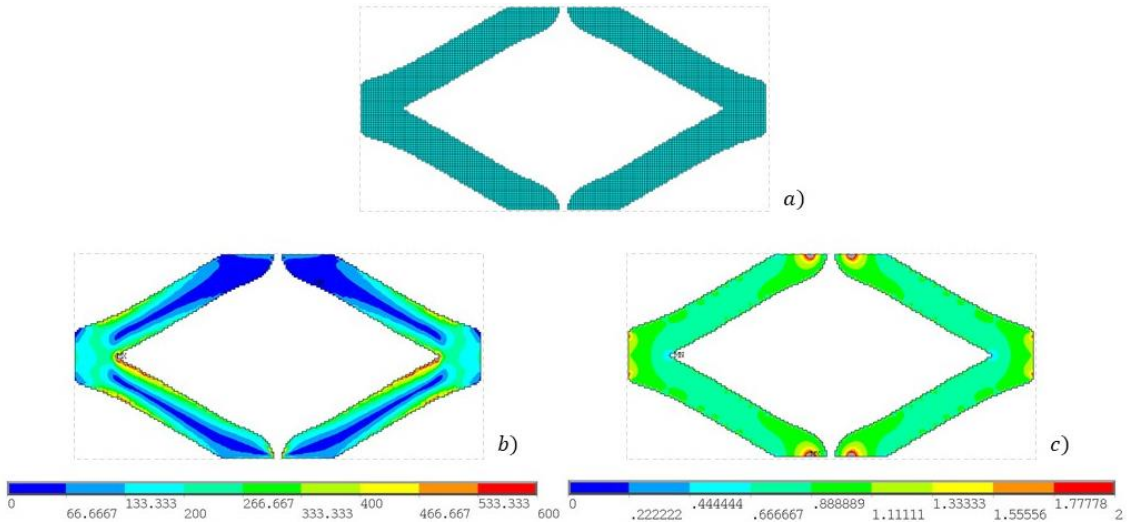

Figure 9 - Meaningful quantities after thermal topology optimisation of load case 1: a) final topology, i.e. material distribution b) Von Mises ideal stress [MPa], c) Thermal gradient vector sum [°C/mm].

Similarly, Fig. (10a) shows the final topology obtained for the load case 2 by considering only the structural reference ($\sigma_{ref} = 120$ MPa), with Fig. (10b) and Fig. (10c) showing the Von Mises stress and the thermal gradient distributions, respectively. The same considerations made for the previous example on load case 1 are applicable. As a matter of fact, Von Mises stresses are well distributed and almost uniform within the domain. On the contrary, the thermal gradient distribution presents remarkable differences in intensity depending on the material zones. Therefore, the heat flows inside the material in a very inefficient way. It is worth to note that the final topology is not identical to the minimum compliance topology optimisation problem for cantilever beam, well known in the literature. This is due to the temperature field inside the domain that modifies the strain distribution. For a precise benchmarking case the reader is referred to Appendix A.

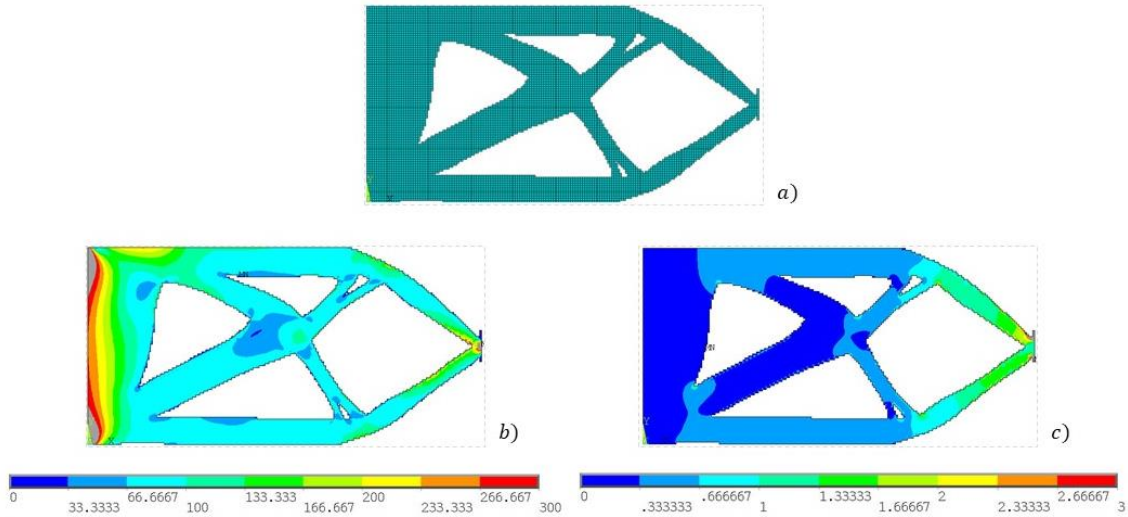

Figure 10 - Meaningful quantities after structural topology optimisation of load case 2: a) final topology, i.e. material distribution b) Von mises ideal stress [MPa], c) Thermal gradient vector sum [°C/mm].

Fig. (11a) shows the thermal topology optimisation carried out on the load case 2, with $\nabla\theta_{ref} = 1.1\ \mathrm{K/mm}$, whereas Fig. (11b) shows the Von Mises stress distribution and Fig. (11c) the thermal gradient sum. In this case the thermal gradient distribution is uniform over the domain providing a very good thermal conduction. In particular, Fig. (11c) shows a very good distribution of the gradient inside the domain. On the contrary, the mechanical task is not considered, and this can be detrimental for the structural integrity.

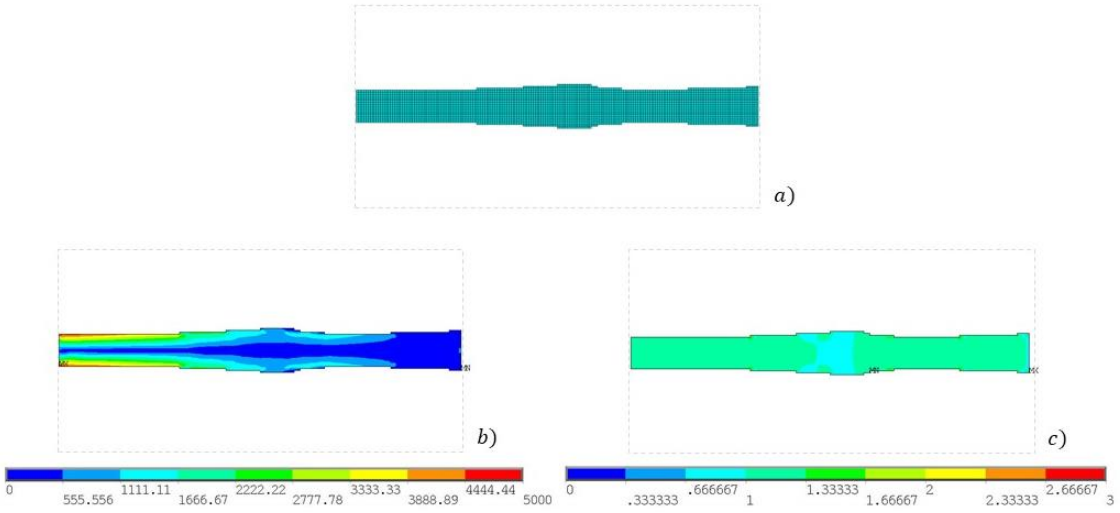

Figure 11 - Meaningful quantities after thermal topology optimisation of load case 2: a) final topology, i.e. material distribution, b) Von Mises ideal stress [MPa], c) Thermal gradient vector sum [°C/mm].

The validation of the proposed algorithm in this Section clearly shows the importance of considering concurrently mechanical and thermal loads, if present, in the topology optimization process. The thermo-mechanical topology optimisation provides the best topology for a component which undergoes coupled constraints and loads, permitting to obtain a uniform distribution of the thermo-mechanical energy density (Fig. (5)). Indeed, the coupled optimisation provides the best compromise between the mechanical and the thermal properties distribution and considers both the contributions, ensuring an optimal material distribution and the least material waste in order to concurrently achieve the best heat conduction and structural performance.

3.2 Thermo-mechanical topology optimization: validation on a real component

In this subsection, the proposed algorithm is applied to a thermo-mechanical real application. In particular, the topology of a radiator for a loop heat pipe (LHP) is optimized. The applied loads and constraints are taken from the literature and data not available have been assumed, with the aim of proving that the proposed thermo-mechanical topology optimisation can be

employed for real components allowing to maximise the performance of components subjected to thermo-mechanical loads.

The radiator of a Titanium Loop Heat Pipes (LHP) for Space Nuclear Power System similar to that analysed in (25) is considered. As shown in Fig. (12), the radiator has a parallelepiped shape with a square base with $L = 305\ \mathrm{mm}$ and height $h = 26.2\ \mathrm{mm}$. Two pipes enter symmetrically in the radiator and exit after three folds each from the same side. The fluid path is also shown in Fig. (12).

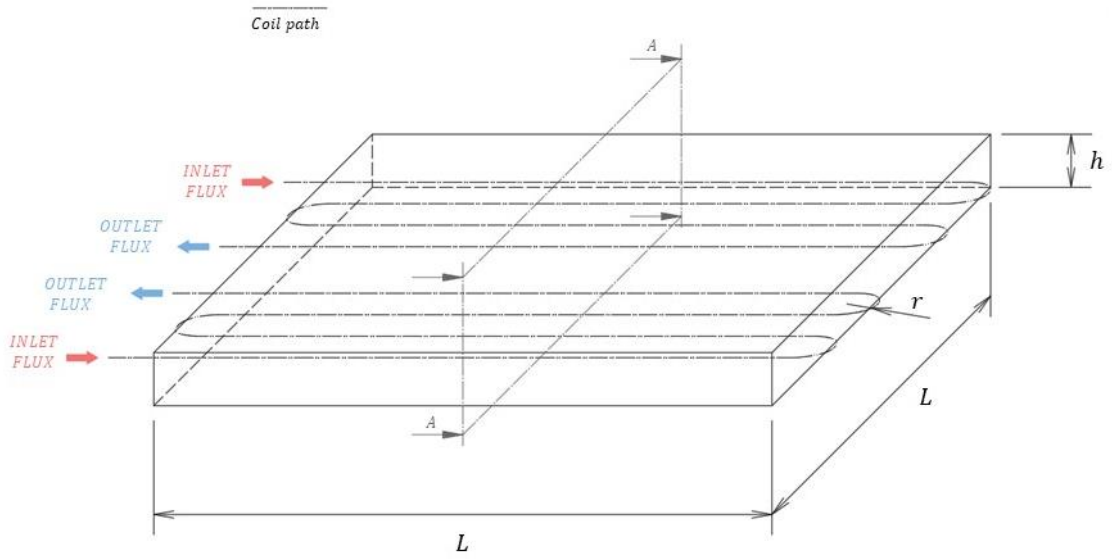

Figure 12 – Radiator model and design domain with dimensions (continue black lines), coil path (dash-dot black line) and flux directions (red and blue arrows).

Considering a cross section A as shown in Fig. (13), it is possible to notice that for each section eight holes are present. They are symmetric with respect to both the axes of the rectangular section. The radius of the pipe is constant all over the radiator and is equal to $R = 9.55\ mm$. Each fold has a radius of $r = 15\ mm$, causing a distance between the pipes inside the domain of $d = 30\ mm$. Given this geometry it is easy to notice that the cross section is constant along the radiator.

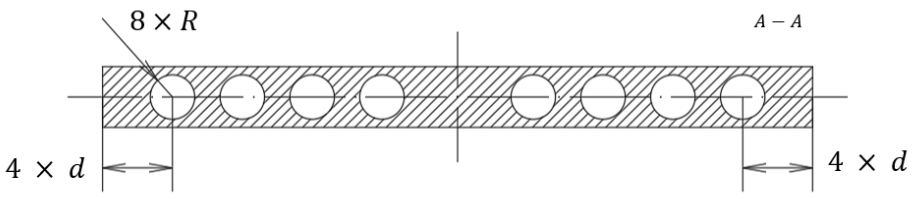

Figure 13 – Cross section A of the radiator from Fig. (12) with dimensions.

The first phase of the optimization process involves the definition of the design and the non-design domain. The heat pipes are in almost all the applications inserted in a sandwich panel,

with the core composed by a honeycomb structure (26). For the redesign of the radiator with the proposed coupled topology optimization algorithm, the honeycomb structure is filled with a single isotropic material (design domain). On the contrary, the dimensions of the cross-section, of the radiator and heat pipes are left unaltered. A Titanium alloy Ti6Al4V, whose mechanical and thermal properties are reported in Table 2, was considered for the redesign and for the production of the component through an AM process (27). Indeed, the complex shape obtained as a result of the optimization process, which can be hardly produced through traditional process, can be more easily produced through an AM manufacturing process.

Material	E [GPa]	ν	ρ [Kg/m^3]	k [W/mK]	α [1/K]
Ti6Al4V	113.8	0.342	4430	6.7	9e-6

Table 2 – Ti6Al4V properties

It is worth to note that the component has a constant cross section, i.e. extrusion symmetry, and the cross section itself presents a double symmetry with respect to its axes. Therefore, for the optimization of the radiator only a quarter of the entire cross section, shown in Fig. (14a), was considered and symmetric boundary conditions were applied. More in detail and by considering the mechanical loads, the radiator is supposed to carry the entire weight of Space Nuclear Power System which it is cooling (28). Usually, the devices which are to be cooled are connected by pots and inserts inside the panels. However, in order to avoid many assumptions and computational complications, the load is uniformly distributed over the surface. In particular, the forces applied on the radiator are defined considering the entire weight of the Space Nuclear Power System multiplied by the average accelerations during the launch phase of the spacecraft (worst possible and conservative condition). The weight of a model of the Power System for this type of radiator is about $M = 56\,kg$, as reported in (29). Commonly the maximum acceleration during launch phase of spacecraft are 20 times the gravity acceleration, g, on Earth. Overall, the forces applied to the quarter of the cross section, Fig. (14b), is the product of the Power System weight and the total acceleration in both directions split by four per unit of length, as reported by Eq. (14):

$$F_x = F_y = \frac{20Mg}{4L} = 9\frac{N}{mm} \tag{14}$$

In addition, internal pressure caused by the fluid inside the pipes is considered. The maximum internal pressure is $p_{int} = 2.63\,MPa$, as reported in (26). For what concern the constraints, the radiator is supposed to be locked all along its lateral sides, as shown in Fig. (14b).

From the thermal point of view Fig. (14c), (26) provides the constant internal temperature of the fluid inside the pipes $\theta = 413K$ and a total absorbed heat $Q_{tot} = 590W$. As for the mechanical field, the inlet heat applied on the portion of cross section is split by four and considered per unit of length as in Eq. (15)

$$Q = \frac{Q_{tot}}{4L} = 0.48\frac{W}{mm} \tag{15}$$

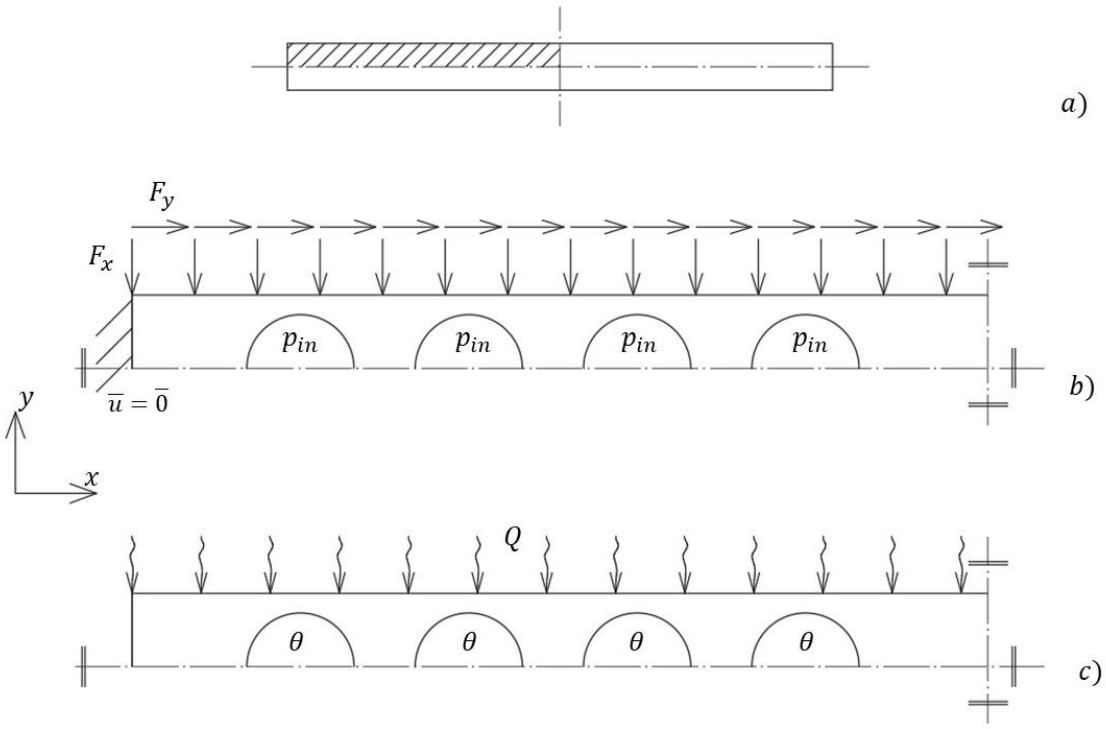

Figure 14 – Loads and constraints applied to redesigned panel: a) selected quarter portion from the entire radiator cross section, b) structural boundary conditions, c) thermal boundary conditions made of incoming heat Q on the upper side and fixed temperature θ inside the pipes.

Given the aforementioned boundary conditions, three different optimisations problems have been set up and the final topologies are shown in Fig. (15). Fig. (15a) shows the result of a structural topology optimisation with a stress reference $\sigma_{ref} = 130\ MPa$. Fig. (15b) shows the result of the thermal topology optimisation with a thermal gradient reference $\nabla\theta_{ref} = 2.5\ K/mm$. Finally, Fig. (15c) shows the final material distribution after the thermo-mechanical topology optimisation with a stress reference of $\sigma_{ref} = 130\ MPa$, a thermal gradient reference of $\nabla\theta_{ref} = 2.5\,K/mm$ and a linker term evaluated as $\xi = \sigma_{ref}^2/Ek\nabla\theta_{ref}^2$. These quantities provide a value of the reference thermo-mechanical energy density $\epsilon_{ref} = 0.149\,MPa$ according to Eq. (13). 14145 plane quad elements, 8 nodes each one, are employed for the analysis.

Figure 15 – Final material distribution after: a) fully thermal topology optimisation, b) fully structural topology optimisation, c) thermo-mechanical topology optimisation.

In order to compare the three optimisation results reported in Fig. (15) and to understand the effectiveness of the coupled method, further analyses have been carried out. Figures 16-19 show the displacement field, the Von Mises stress distribution, the temperature field, and the thermal gradient vector sum distribution respectively within the three different final topologies. Each topology is reported together with a letter index and in particular: subscript *a)* refers to the pure thermal optimisation, subscript *b)* refers to the pure mechanical optimisation and subscript *c)* refers to the coupled optimisation. The same considerations made on the simple cases analysed in the previous subsection are still valid. Observing the displacement vector sum in Fig. (16), it is clear that the pure thermal topology optimisation is not able to predict the structural load causing an enormous displacement, i.e. the component would be broken. Looking at the other final topologies (17b, 17c), the displacement vector sum is always less or much less than 0.1 mm which can be considered an acceptable value for the analysed geometries, proving the verification of the structural constrains. The validity of this consideration is enhanced if the Von Mises stress distribution is observed in Fig. (17). This quantity in the thermal optimisation presents great underloaded portions and other with stress peaks, i.e. it is highly irregular and ununiform. On the contrary, in the pure mechanical optimisation (17b) and in the coupled one (17c) this quantity is almost uniform within the final domain, especially in the pure mechanical optimisation as expected.

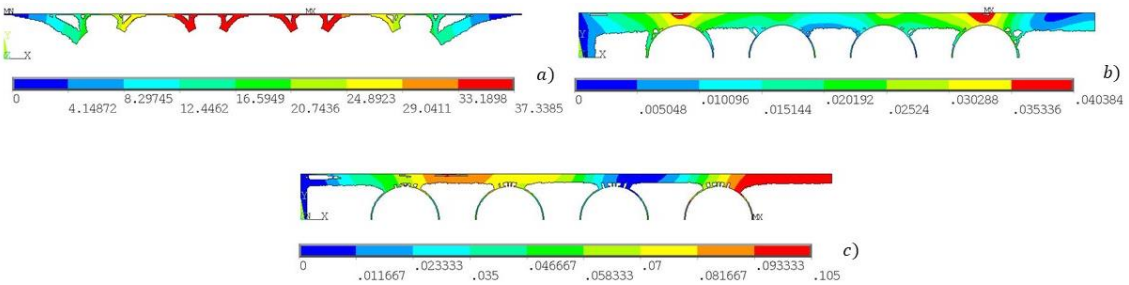

Figure 16 – Displacement vector sum distribution [mm], a) thermally optimised domain b) structurally optimised domain c) thermo-mechanically optimised domain.

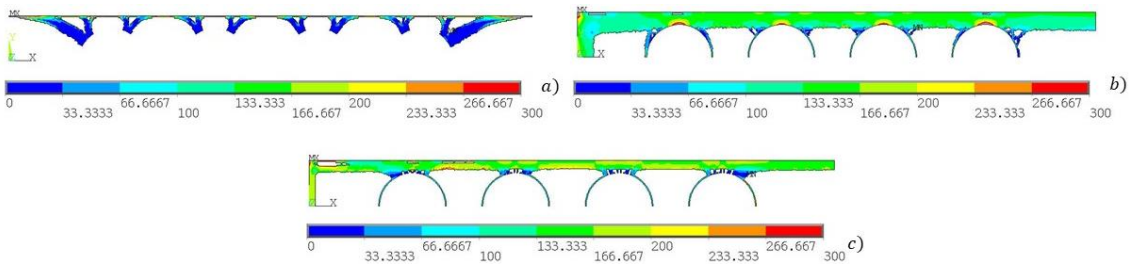

Figure 17 –Von Mises ideal stress distribution [MPa], a) thermally optimised domain b) structurally optimised domain c) thermo-mechanically optimised domain.

Similarly, looking at the temperature field Fig. (18) and the thermal gradient vector sum distribution Fig. (19), it is clear that the mechanical optimisation alone is not able to provide a good result. In particular, in the pure thermal optimisation, Fig. (18a), the temperature fluctuations inside the domain are low. In the other optimisations, Figures (18b, 18c), the temperature undergoes more dispersions. For more, looking at the thermal gradient vector sum distribution of the thermal optimisation Fig. (19a) it is incredibly uniform within this final domain, while is highly scattered in the mechanical in Fig. (19b). However, in the couple optimisation Fig. (19c) it is well distributed, a good compromise between the two extreme optimisations.

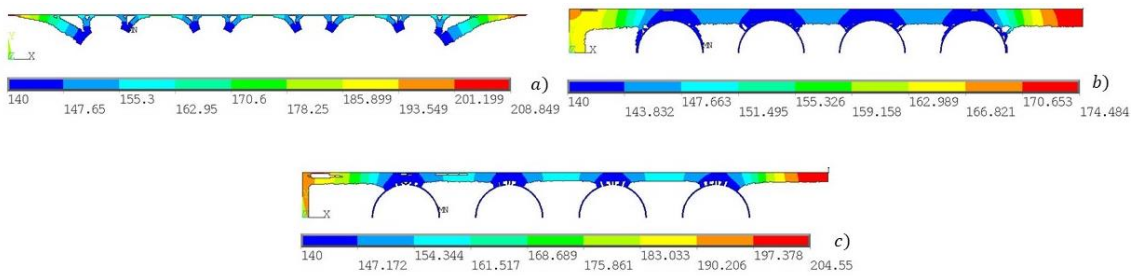

Figure 18 –Temperature field [°C], a) thermally optimised domain b) structurally optimised domain c) thermo-mechanically optimised domain.

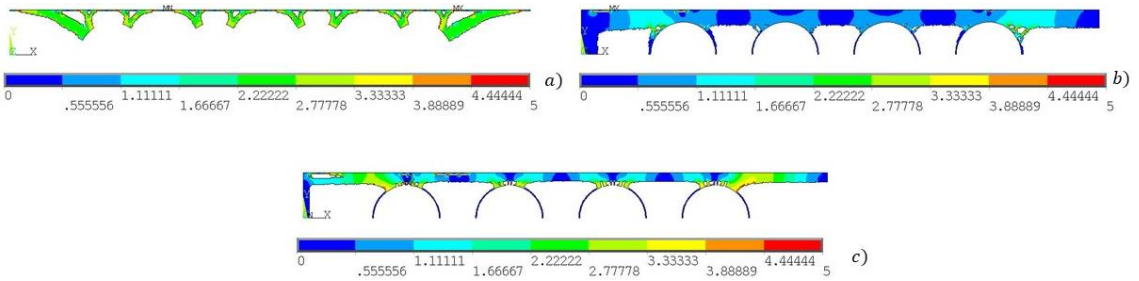

Figure 19 –Thermal gradient vector sum distribution [°C /mm], a) thermally optimised domain b) structurally optimised domain c) thermo-mechanically optimised domain.

As a matter of fact, it is evident that the coupled optimisation is able to provide the best compromise between the two different limit conditions. In other words, it is able to provide a final topology in which no constraint is neglected, and heat exchange and structural stiffness are concurrently optimised. The same consideration cannot be made on the single optimisation cases, in fact the structural optimisation provides very poor result in terms of heat exchange, with disperse thermal gradient. Similarly, the single thermal optimisation leads to unfeasible topology under the mechanical loads.

Fig. (20) displays the distribution of the thermo-mechanical energy density that is almost uniform around the reference value of ϵ_{ref}. Overall, the coupled potential energy has been spread equally in the optimised structure, in accord with the analytical formulation, while stress and thermal gradient find in this topology the best compromise.

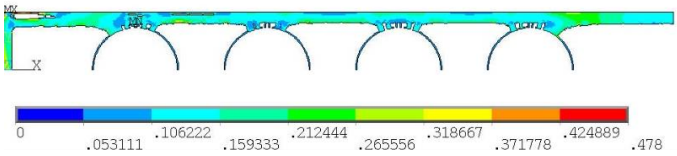

Figure 20 – Thermo-mechanical energy density distribution on final domain obtained by coupled optimisation [MPa].

In order to highlight the potentialities of the proposed coupled algorithm, Table 3 compares important quantities evaluated for the three final structures. The first row displays the maximum temperature θ_{max} within the domain whereas the second the maximum displacement vector sum $\overline{u}_{max}$. The third and the fourth rows show the final mass M_{opt} per quarter of section and as a percentage with respect to the initial quarter cross section mass, $M_{opt\%}$. The mechanical stiffness, S^u, the mechanical stiffness per unit of mass, s^u, the thermal stiffness, S^θ, and the thermal stiffness per unit of mass, s^θ, defined in Eq. (16), are also reported in the last four rows of Table 3, respectively.

$$S^u = \frac{\sqrt{F_x^2 + F_y^2}}{\overline{u}_{max}}; \quad s^u = \frac{S^u}{M_{fin}}$$
$$S^\theta = \frac{Q}{\theta_{max}}; \quad s^\theta = \frac{S^\theta}{M_{fin}} \tag{16}$$

	$Thermal\ opt.$	$Mechanical\ opt.$	$Thermo-mechanical\ opt.$
$\theta_{max}\ [°C]$	209	175	205
$\overline{u}_{max}\ [mm]$	37,339	0,040	0,105
$M_{opt}\ [g/mm]$	1,02	3,47	1,92
$M_{opt\%}\ [\%]$	16%	55%	30%
$S^\theta [Wmm^{-1}°C^{-1}]$	0,0023	0,0028	0,0024
$s^\theta [Wmm^{-1}°C^{-1}\ kg^{-1}]$	2,269	0,796	1,229
$S^u [Nmm^{-2}]$	0,34	318,20	121,22
$s^u [Nmm^{-2}kg^{-1}]$	337	91700	63135

Table 3 – Comparison between optimisation results

According to Table 3, the temperature and the displacement after the mechanical optimization are the smallest, but the mass is significantly larger (more than 3 times M_{opt} obtained through thermal optimization and more than twice M_{opt} after the coupled thermo-mechanical optimization). By considering the thermal optimisation, it is clear that this solution is not feasible, since the displacement is out of scale, i.e. the component would break immediately under the structural loads. On the contrary, the displacement and the temperature in the coupled solution are reasonable and a good compromise between the separated optimisations. In addition, M_{opt} results to be remarkably smaller than M_{opt} obtained through a mechanical optimization. Moreover, the stiffnesses per unit of mass are concurrently enhanced after the coupled optimisation and tend to the values obtained by considering only the mechanical and the thermal optimisations (i.e., the highest achievable performances). It is worth to note that the thermal peak in the pure thermal topology optimisation is localised in a very little portion of material, as shown in Fig. (18a), about just one or two elements. In order to have a rigorous comparison between all the optimisation, this value has been reported unaltered from the analysis. However, it would be sufficient to add a very little quantity of material in that point to remarkably reduce the temperature peak that is mainly due to a numerical instability. As already pointed out, the presented final topologies depend on the reference stress σ_{ref} and on reference thermal gradient $\nabla\theta_{ref}$ prescribed at the beginning of the optimisation. In the present paper, qualitatively high values of these references have been employed to show clearly the effect of the optimisation and highlight the most critical zones in the component. Surely, in a real design phase, these references can be lowered, and the final mass would be much more

increased. To conclude, this validation on a real component proves furthermore that the proposed thermo-mechanical topology optimisation algorithm is able to provide the optimized comprise between the structural and the thermal constraints, providing a final topology characterized by high structural and thermal performances and reduced mass.

In Fig. (21) the final radiator is displayed. In particular, the figure shows an internal section of the radiator in order to highlight the redesigned topology and proving that topology obtained with the proposed optimization topology can be easily converted in a CAD file. Nevertheless, the proposed final topology doesn't consider manufacturability constraints. As it can be noticed, the great mass removal especially close to the cooling channels may be problematic in the manufacturing phase. It is worth to note that, as for other commercial software for topology optimization, the manufacturing constraints have not been considered, since the aim of topology optimization is to provide the ideal mass distribution under selected loads and constraints. Considerations on the specific manufacturing limits and constraints have to be faced during the rebuilding of the model. Indeed, topology optimisation provides a guideline about the best material distribution within a certain domain and under some constraints and boundary conditions.

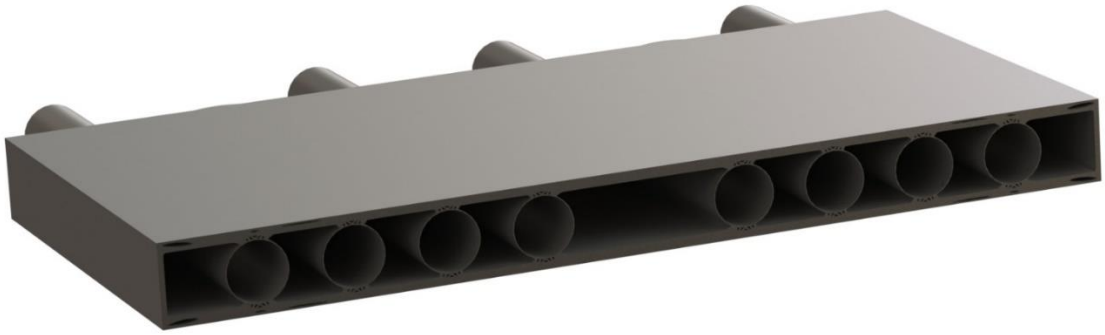

Figure 21 – Section of radiator optimized with the thermo-mechanical topology optimisation.

In order to give the most possible generality to the algorithm, in the presented paper manufacturing technique references have been omitted. Nevertheless, for components subjected to a topology optimization process the most suitable production process is Additive Manufacturing (AM). This is because AM processes are capable to produce really complex shape such as those provided by the topology optimisation design. The reader is referred to Meng et al. (30) for a deeper analysis of the connection between AM and Topology optimisation. Therefore, it is of outmost interest to include in the topology optimisation algorithm possible

constraints specific of the AM process. Just to mention some of them, inhomogeneous distribution of materials and composition, over angles, process anisotropy and so on. The reader can find a review about this type of constrain in Liu et al. (31). Further improvements of the presented algorithm may include this type of constraints in order to facilitate the production through AM techniques.

CONCLUSIONS

In the literature, components subjected to mechanical and thermal loads are generally optimized with separate mechanical and thermal optimizations. Moreover, in many cases thermal loads are not considered and only structural topology optimization is carried out. In the paper, a methodology to define the optimized structure under simultaneous thermo-mechanical constraints is proposed. The mathematical formulation of the presented method is shown and is validated on several application examples. The main conclusions can be summarized as follows:

1) The theoretical condition for the optimum consists in the uniform energy density distribution, with the convergence reached within few iterations. In all analysed cases full or void material distribution without intermediate properties has been achieved after about 40 iterations.
2) The proposed methodology permits to obtain the maximum material exploitation, reaching the optimized heat exchange and stiffness concurrently. Indeed, for a component subject to coupled loads, this algorithm is able to provide the best compromise, optimising concurrently the above-mentioned quantities and respecting the coupled constraints.
3) The algorithm has been successfully validated on an LHC radiator for aerospace application, proving its applicability in real and complex cases. As it can be observed from the reported data, within the final structure, the heat exchange and the structural stiffness are maximised. From the topology optimisation result, it had been possible to redesign entirely the component quite easily. Hence, it had been possible to obtain a CAD model, first step in the manufacturing chain.

Therefore, the proposed methodology represents a useful tool for the redesign of components subjected to thermo-structural loads.

To conclude, the proposed algorithm and AM processes can produce components characterized by enhanced mechanical and thermal performances together with a significant mass reduction.

APPENDIX: A

In the following section, two comparative benchmarks for thermal and structural topology optimisation are provided, with the aim of showing that the proposed algorithm works properly also for simple cases, like as heat conduction and compliance minimisation topology optimisation considered separately. Indeed, it is worth to note that, if the thermal or mechanical energy density is null, the algorithm works as purely structural or thermal topology optimization respectively.

In Fig. A1 the thermal model of the heat condition topology optimisation problem is presented. It is a square domain with a portion of the left side at a fixed temperature. In the whole domain a heat generation rate is imposed. This example has been taken from (32) page 271. For the details on the numerical implementation, boundary conditions and the material the reader is referred to the detailed description in (32).

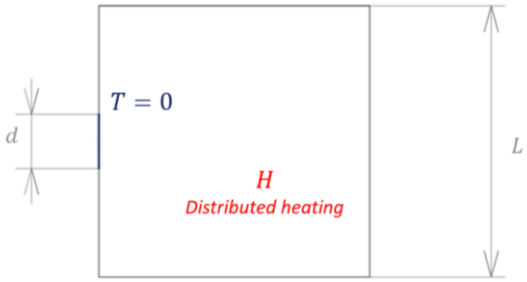

Figure A1 –Thermal boundary conditions and geometry settings.

In Fig. A2 the results are shown. In particular Fig. A2a shows the result achieved by (32) while Fig. A2b shows the result obtained with the presented algorithm. As it can be noticed, the two results are almost identical. It is worth to note that with the proposed method no intermediate densities have been found in the final structure.

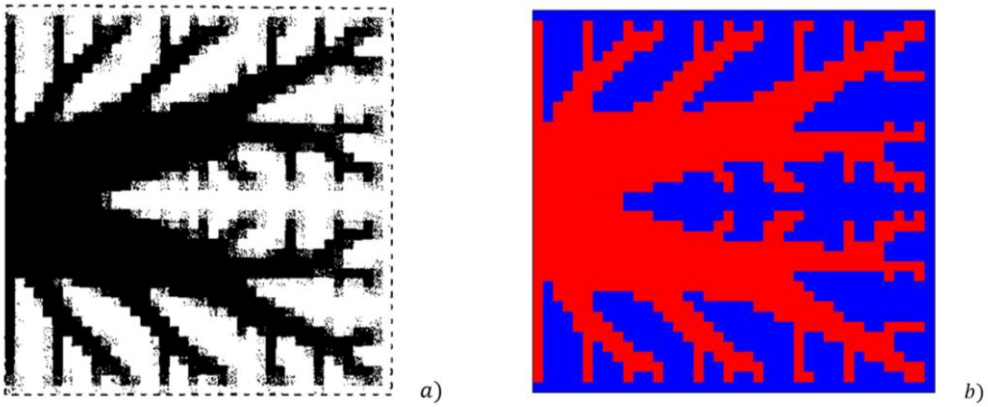

Figure A2 – Heat conduction topology optimisation: a) Final topology (in black) from (32), b) Final topology (in red) obtained with the proposed algorithm.

In Fig. A3 the structural model of minimum compliance topology optimisation is presented. It is a rectangular domain with the left side fully constrained and a nodal downwards vertical force on the right lower vertex. This example has been taker from (24) page 123 Fig. (2). As for the thermal benchmark, the same data has been used to reproduce the results with the proposed algorithm. Again, for the details on the numerical implementation, boundary conditions and material the reader is referred to the detailed description in (24).

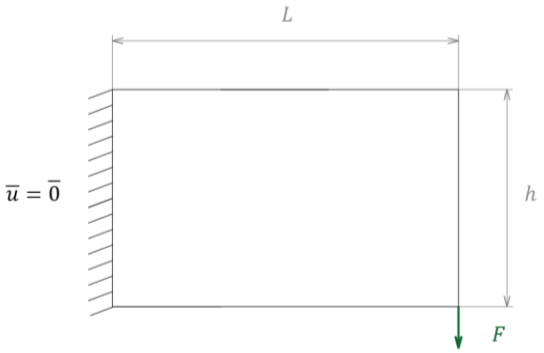

Figure A3 – Structural boundary conditions and geometry settings.

Fig. A4 shows the comparative results. In detail, Fig. A4a is the results achieved by (24) while Fig. A4b reports the result obtained with the presented algorithm. As it can be noticed the two results are almost identical as for the thermal benchmark, but no intermediate densities have been found in the final structure with the proposed methodology.

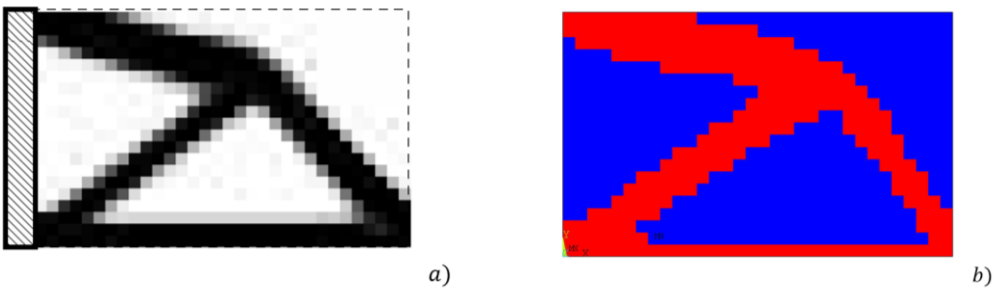

Figure A4 – Compliance minimisation topology optimisation: a) Final topology (in black) from (24), b) Final topology (in red) obtained with the proposed algorithm.

These two benchmarks proved the effectiveness of the proposed formulation even for simple cases.

REFERENCES

1. Bendsøe MP, Sigmund O. Material interpolation schemes in topology optimization. Arch Appl Mech (Ingenieur Arch. 1999 Nov 22;69(9–10):635–54.
2. Huang X, Xie YM. Bi-directional evolutionary topology optimization of continuum structures with one or multiple materials. Comput Mech. 2009;43(3):393–401.
3. Van Dijk NP, Maute K, Langelaar M, Van Keulen F. Level-set methods for structural

topology optimization: A review. Struct Multidiscip Optim. 2013;48(3):437–72.
4. Sigmund O, Maute K. Topology optimization approaches: A comparative review. Struct Multidiscip Optim. 2013;48(6):1031–55.
5. Dbouk T. A review about the engineering design of optimal heat transfer systems using topology optimization. Appl Therm Eng. 2017;112:841–54.
6. Subramaniam V, Dbouk T, Harion JL. Topology optimization of conductive heat transfer devices: An experimental investigation. Appl Therm Eng. 2018;131:390–411.
7. Gersborg-Hansen A, Bendsøe MP, Sigmund O. Topology optimization of heat conduction problems using the finite volume method. Struct Multidiscip Optim. 2006;31(4):251–9.
8. Gao T, Zhang WH, Zhu JH, Xu YJ, Bassir DH. Topology optimization of heat conduction problem involving design-dependent heat load effect. Finite Elem Anal Des. 2008;44(14):805–13.
9. Zhu X, Zhao C, Wang X, Zhou Y, Hu P, Ma ZD. Temperature-constrained topology optimization of thermo-mechanical coupled problems. Eng Optim. 2019;51(10):1687–709.
10. Gao T, Xu P, Zhang W. Topology optimization of thermo-elastic structures with multiple materials under mass constraint. Comput Struct. 2016;173:150–60.
11. Deaton JD, Grandhi R V. Stress-based design of thermal structures via topology optimization. Struct Multidiscip Optim. 2016;53(2):253–70.
12. Zhang W, Yang J, Xu Y, Gao T. Topology optimization of thermoelastic structures: Mean compliance minimization or elastic strain energy minimization. Struct Multidiscip Optim. 2014;49(3):417–29.
13. Liu X, Wang C, Zhou Y. Topology optimization of thermoelastic structures using the guide-weight method. Sci China Technol Sci. 2014;57(5):968–79.
14. Yang Q, Gao B, Xu Z, Xie W, Meng S. Topology optimisations for integrated thermal protection systems considering thermo-mechanical constraints. Appl Therm Eng. 2019;150:995–1001.
15. Takezawa A, Yoon GH, Jeong SH, Kobashi M, Kitamura M. Structural topology optimization with strength and heat conduction constraints. Comput Methods Appl Mech Eng. 2014;276:341–61.
16. Krysko A V., Awrejcewicz J, Pavlov SP, Bodyagina KS, Krysko VA. Topological optimization of thermoelastic composites with maximized stiffness and heat transfer. Compos Part B Eng. 2019;158:319–27
17. Deng X, Wang J, Zhou J, Shen H, Sheng Z, Zhang J, et al. A hybrid cellular automaton method for structural topology optimization with mechanical and heat constraints. Front Heat Mass Transf. 2019;12.
18. Sigmund O, Petersson J. Numerical instabilities in topology optimization: A survey on procedures dealing with checkerboards, mesh-dependencies and local minima. Struct Optim. 1998;16(1):68–75.
19. K. Svanberg. The method of moving asymptotes - a new method for structural optimization. Int J Numer Methods Eng. 1987;24(2):359–73.
20. Marsden JE, Hughes TJ. Mathematical Foundations of Elasticity. Dover publications, Inc. New York. 1994.
21. Codegone M, Sanchez-Palencia E. Asymptotics ofthe scattering frequencies for a thermoelasticity problem with small thermal conductivity. Modélisation mathématique Anal numérique. 1989;23(1):87–101.
22. Caivano R, Tridello A, Paolino D, Chiandussi G. Topology and fibre orientation simultaneous optimisation: A design methodology for fibre-reinforced composite components. Proc Inst Mech Eng Part L J Mater Des Appl. 2020;234(9):1267–79.
23. Chiandussi G. On the solution of a minimum compliance topology optimisation problem by optimality criteria without a priori volume constraint specification. Comput Mech. 2006;38(1):77–99.
24. Sigmund O. A 99 line topology optimization code written in matlab. Struct Multidiscip

Optim. 2001;21(2):120–7.
25. Hartenstine JR, Anderson WG, Bonner R. Titanium loop heat pipes for space nuclear power systems. AIP Conf Proc. 2008;969:44–52.
26. Anderson WG, Bonner R, Hartenstine J, Barth J. High temperature titanium-water heat pipe radiator. AIP Conf Proc. 2006;813:91–9.
27. Dutta B, Froes FH. The Additive Manufacturing (AM) of titanium alloys. Metal Powder Report 2017;72:96–106.
28. Boudjemai A, Bouanane MH, Mankour A, Salem H, Hocine R, Amri R. Thermo-mechanical design of honeycomb panel with fully-potted inserts used for spacecraft design. RAST 2013 - Proc 6th Int Conf Recent Adv Sp Technol. 2013;39–46.
29. Sanchez-Torres A. Radioisotope Power Systems for Space Applications. Radioisot - Appl Phys Sci. 2011.
30. Meng L, Zhang W, Quan D, Shi G, Tang L, Hou Y, et al. From Topology Optimization Design to Additive Manufacturing: Today's Success and Tomorrow's Roadmap. Arch Comput Methods Eng. 2020;27(3):805–30.
31. Liu J, Gaynor AT, Chen S, Kang Z, Suresh K, Takezawa A, et al. Current and future trends in topology optimization for additive manufacturing. Struct Multidiscip Optim. 2018;57(6):2457–83.
32. Bendsøe MP, Sigmund O. Topology Optimization: Theory, Methods and Applications. Springer, editor. Springer. 2002.